

Using Deformable Models for the Localization of 3D Anatomical Point Landmarks in 3D Tomographic Images*

Sönke Frantz¹, Karl Rohr², and H. Siegfried Stiehl¹

¹Universität Hamburg, Fachbereich Informatik, Arbeitsbereich Kognitive Systeme, Vogt-Kölln-Str. 30, 22527 Hamburg frantz@informatik.uni-hamburg.de

²Internat. University in Germany, School of Information Technology, 76646 Bruchsal

Abstract. This paper describes a new approach to the localization of 3D anatomical point landmarks in 3D tomographic images on the basis of deformable models. It is demonstrated that compared to a purely differential approach, the localization accuracy is improved and also the number of false detections is reduced.

1 Introduction

We consider the problem of extracting 3D anatomical point landmarks from 3D tomographic images of the human head. The driving task is 3D image registration, which is fundamental to computer-assisted neurosurgery. Only a few (semi-)automatic differential approaches for extracting 3D point landmarks exist (e.g., [1, 2, 3]). A common problem with such, rather local, approaches is their sensitivity to noise. As a consequence, the localization accuracy is affected in a negative way and false detections occur. This paper describes a new approach to 3D landmark localization on the basis of deformable models, which takes into account more global image information in comparison to differential approaches and thus allows to alleviate the aforementioned problems. In medical image analysis, deformable models have been primarily used for object segmentation and tracking as well as for image-atlas matching (see [4] for a survey). However, the localization of 3D point landmarks on the basis of deformable models has not been considered so far.

Exemplarily, we focus on two different types of 3D point landmarks, viz., salient surface loci (curvature extrema) of tip- and saddle-like structures. Examples of such landmarks in the case of the human head are the tips of the ventricular horns (see Fig. 1) or the saddle points at the zygomatic bones. To describe such structures, we utilize 3D surface models. In the literature, a wide variety of surface models has been used (see, e.g., [4]). Note, however, that in contrast to earlier work on deformable models, we are here interested in the accurate localization of salient surface loci. Central to an efficient solution of this specific problem is that the model surface exhibits a unique point whose position can be directly computed from the model parameters. Addressing this problem, we use quadric surfaces as 3D shape prototypes, which additionally undergo global deformations such as to enlarge the range of shapes. The problem of landmark localization is thus reduced to the problem of finding optimal parameter values for describing the structure at hand in the 3D image data.

* This work was supported by Philips Research Hamburg, project IMAGINE.

2 Geometric Models of Tip- and Saddle-Like Structures

Tip-like structures. As 3D shape prototype, we consider a (half-)ellipsoid. To cope with bended structures such as the ventricular horns, the prototype undergoes a bending deformation \mathcal{B} along the z -axis ([6]), $\mathcal{B}(\mathbf{x}) = (x + \delta z^2 \cos v, y + \delta z^2 \sin v, z)^T$, where δ determines the strength and v the direction of bending. Finally, to transform from object-centered coordinates to image coordinates, we apply a rigid transformation $\mathcal{R}(\mathbf{x}) = \mathbf{R}\mathbf{x} + \mathbf{t}$, where $\mathbf{t} = (X, Y, Z)^T$ denotes the translation vector and \mathbf{R} the rotation matrix depending on the rotation angles α, β, γ . The parametric form of our model thus reads

$$\mathbf{x}_{\text{tip}}(\theta, \phi) = \mathcal{R} \circ \mathcal{B} \circ (a_1 \cos \theta \cos \phi, a_2 \cos \theta \sin \phi, a_3 \sin \theta)^T, \quad (1)$$

where $0 \leq \theta \leq \pi/2$ and $-\pi \leq \phi < \pi$ are the latitude and longitude angle parameters, resp., and $a_1, a_2, a_3 > 0$ are scaling parameters. Hence, the model is fully described by the parameter vector $\mathbf{p}_{\text{tip}} = (X, Y, Z, \alpha, \beta, \gamma, a_1, a_2, a_3, \delta, v)$. The landmark position of our model, i.e., the position of the curvature extremum of the deformed ellipsoid, is given by $\mathbf{x}_1 = \mathbf{x}_{\text{tip}}(\pi/2, 0) = \mathbf{R}(\delta a_3^2 \cos v, \delta a_3^2 \sin v, a_3)^T + \mathbf{t}$ (see Fig. 2 (left) for an example of a bended tip-like structure).

Saddle-like structures. Here, a (half-)hyperboloid of one sheet serves as 3D shape prototype. In addition, the prototype is rotated and translated:

$$\mathbf{x}_{\text{saddle}}(\theta, \phi) = \mathcal{R} \circ (a_1 \cos \phi / \cos \theta, a_2 \sin \phi / \cos \theta, a_3 \tan \theta)^T, \quad (2)$$

where $|\theta| < \pi/2$ and $0 \leq \phi \leq \pi$. In this case, the model is fully described by $\mathbf{p}_{\text{saddle}} = (X, Y, Z, \alpha, \beta, \gamma, a_1, a_2, a_3)$. The landmark position is here given by $\mathbf{x}_1 = \mathbf{x}_{\text{saddle}}(0, \pi/2) = \mathbf{R}(0, a_2, 0)^T + \mathbf{t}$ (see Fig. 2 (right) for an example).

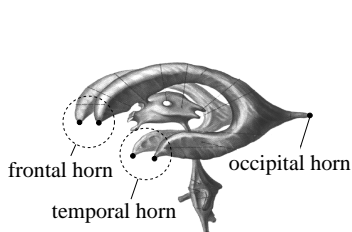


Fig. 1. Ventricular system of the human brain (from [5]).

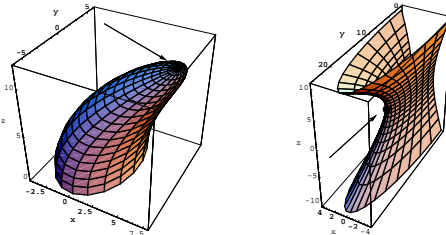


Fig. 2. Geometric models based on quadric surfaces as 3D shape prototypes.

3 Fitting the Geometric Models to the 3D Image Data

Model fitting is formulated as an optimization problem where a suitable fitting measure is optimized w.r.t. the model parameters. Here, we consider an edge-based fitting measure. Our fitting measure is a 3D generalization of the 2D fitting measure in [7] and exploits (a) the similarity between the directions of the intensity gradient and the normals of the model surface and (b) the strength of the intensity variations (a similar 3D fitting measure was used in [8]).

During fitting, we consider the contribution of the intensity gradient in the direction of the normal of the model surface:

$$M_{\text{fit}}(\mathbf{p}) = \pm \iint_{\theta, \phi} \langle \nabla g(\mathbf{x}(\theta, \phi; \mathbf{p})), \frac{\partial \mathbf{x}(\theta, \phi; \mathbf{p})}{\partial \theta} \times \frac{\partial \mathbf{x}(\theta, \phi; \mathbf{p})}{\partial \phi} \rangle d\phi d\theta \rightarrow \min., \quad (3)$$

where g is the intensity function, \mathbf{x} denotes the parametric form of the respective geometric model depending on θ, ϕ , and the model parameter vector \mathbf{p} , and $\langle \cdot, \cdot \rangle$ is the inner product. The sign \pm in (3) depends on the appearance of the structure at hand in the image: In the case of a dark (bright) structure compared to the surrounding, the sign is positive (negative). We minimize the fitting measure in (3) w.r.t. \mathbf{p} by applying the conjugate gradient method.

Initial values for the model parameters are determined by a differential approach. For tip-like structures, we consider an ellipsoid as approximation. In the case of saddle-like structures, we restricted ourselves to an undeformed hyperboloid of one sheet. Thus, for both models from Sect. 2, we have to find initial values for nine parameters ($X, Y, Z, \alpha, \beta, \gamma, a_1, a_2, a_3$). An initial estimate $\hat{\mathbf{x}}_1$ of the landmark position is obtained by a semi-automatic differential approach ([2, 3]). To initialize the rotation angles α, β, γ , we utilize the direction of the intensity gradient (estimate of the normal) as well as the principal directions of the isointensity surface at $\hat{\mathbf{x}}_1$ (see, e.g., [9, 1] for isointensity surface curvature computation). The scaling parameters a_1, a_2, a_3 are initialized based on the principal curvatures κ_1, κ_2 of the isointensity surface at $\hat{\mathbf{x}}_1$. Note, however, that we have only two principal curvatures, while we have three scaling parameters. To cope with this problem, we here initialize one scaling parameter manually.

4 Experimental Results and Discussion

In this section, we present experimental results of applying our new approach to different anatomical landmarks of the human head in 3D tomographic images.

Tip-like structures. We considered the tips of the frontal and occipital ventricular horns in a 3D T1-weighted MR image. Fig. 3 exemplarily shows the results obtained for the left frontal ventricular horn. The initialization result is depicted in Fig. 3a. Here, the translation parameters X, Y, Z , the rotation angles α, β, γ , and the scaling parameters a_1, a_2 were automatically determined (see Sect. 3); only the scaling parameter a_3 was manually initialized. Given the relatively large number of parameters, model fitting was then performed in two steps for reasons of robustness: To achieve a coarse adaption, we first fitted only the six parameters of the rigid transformation, while the other parameters were kept constant. In the second step, all parameters (translation, rotation, scaling, and bending) were considered during optimization. To diminish the influence of neighboring structures, model fitting was restricted to a spherical region-of-interest (ROI) centered at the estimated landmark position. The fitting result for the left frontal horn is shown in Fig. 3b, while Fig. 3c depicts the localized landmark position, which was directly obtained from the fitting result. For the other landmarks, we obtained similar results.

Saddle-like structures. Here, we considered the saddle points at the zygomatic bones in the same 3D T1-weighted MR image and in addition in a 3D CT image (same patient). In both modalities, we obtained reasonable initial

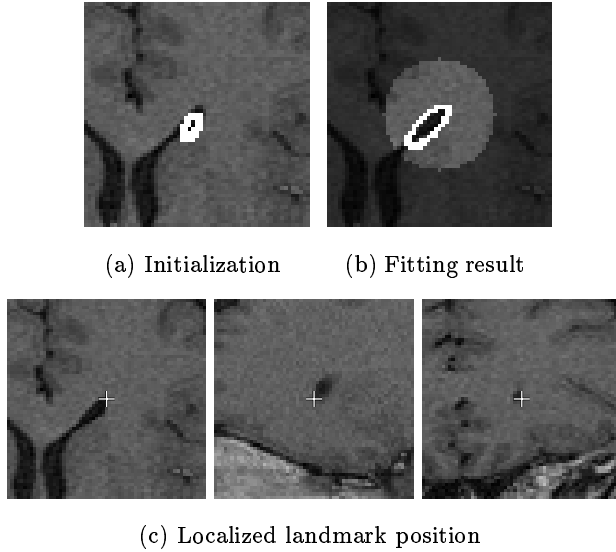


Fig. 3. Localization of the tip of the left frontal ventricular horn in a 3D T1-weighted MR image. (a) and (b) Axial image sections at the ROI center (the considered spherical ROI for model fitting is highlighted in (b)). (c) Orthogonal image sections at the localized landmark position obtained from the fitting results.

values for the model parameters. Only the scaling parameters were manually coarsely initialized. In contrast to the experiments using the ventricular horns, we here performed model fitting in a single step in which all parameters were simultaneously optimized. Fig. 4 shows the localized landmark position for the saddle point at the left zygomatic bone in MR and CT. Similar results were obtained for the saddle point at the right zygomatic bone.

Localization accuracy. To assess the localization accuracy of our new approach, we use as ground truth positions that were manually specified in the 3D MR image in agreement with up to four persons. For the six landmarks in the MR image, the mean Euclidean distance from the positions localized by our new approach to the ground truth positions was $\bar{\epsilon}_{\text{new}} = 1.22\text{mm}$. In comparison, a purely differential approach ([2, 3]), which was here also used to determine initial estimates of the landmark positions, yielded a mean error of $\bar{\epsilon}_{\text{differential}} = 2.11\text{mm}$. Thus, the localization accuracy was improved by 0.89mm.

False detections. One problem with differential approaches is that often more than one landmark candidate is detected, i.e., we have to ensure that a correct candidate is selected for model initialization. To this end, we studied the suitability of using the fitting results to automatically identify false detections. For each landmark from above, we used *all* detected candidates to determine a set of initial values for the model parameters: For the left and right frontal ventricular horn as well as for the right occipital horn in the MR image we obtained two candidates, while for the left (right) zygomatic bone in the MR image we obtained three (five) candidates. In the case of the other landmarks, only one

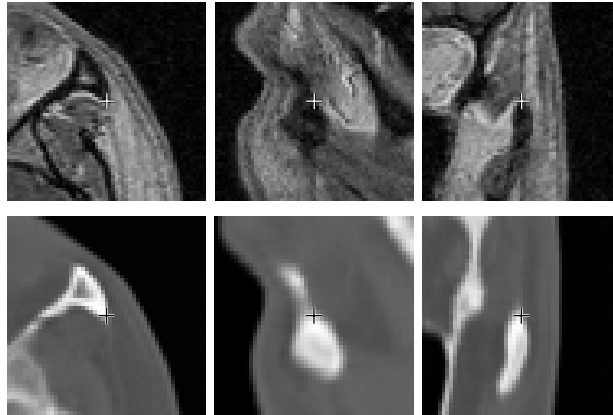


Fig. 4. Localization of the saddle point at the left zygomatic bone in a 3D T1-weighted MR image (top) and a 3D CT image (bottom). Orthogonal image sections at the localized landmark position obtained from the fitting results.

correct candidate was detected. We then compared the fitting results obtained for each candidate based on the value of the fitting measure (3) divided by the surface area (the normalization was done to avoid a bias due to the surface area). We found that in all cases but one, the selection of a correct candidate actually resulted in the best fitting result. For the right occipital horn, it turned out that the detected two candidates are both correct in the sense that they refer to two prominent anatomical loci at the tip of the occipital horn.

In summary, it turned out that compared to a purely differential approach to landmark extraction, the combination of our new approach on the basis of deformable models with a differential approach (for model parameter initialization) improves both the localization accuracy and the detection performance.

References

1. J.-P. Thirion. New Feature Points based on Geometric Invariants for 3D Image Registration. *Internat. Journal of Computer Vision*, 18(2):121–137, 1996.
2. K. Rohr. On 3D differential operators for detecting point landmarks. *Image and Vision Computing*, 15(3):219–233, 1997.
3. S. Frantz et al. Improving the Detection Performance in Semi-automatic Landmark Extraction. In *Proc. MICCAI'99*, pp. 253–262. Springer-Verlag, 1999.
4. T. McInerney and D. Terzopoulos. Deformable Models in Medical Image Analysis: A Survey. *Medical Image Analysis*, 1(2):91–108, 1996.
5. J. Sobotta. *Atlas der Anatomie des Menschen. Band 1: Kopf, Hals, obere Extremität, Haut*. Urban & Schwarzenberg, 19th edition, 1988.
6. K. Delibasis and P.E. Undrill. Anatomical object recognition using deformable geometric models. *Image and Vision Computing*, 12(7):423–433, 1994.
7. M. Worring et al. Parameterized feasible boundaries in gradient vector fields. In *Proc. IPMI'93*, pp. 48–61. Springer-Verlag, 1993.
8. L. Floreby et al. Boundary Finding Using Fourier Surfaces of Increasing Order. In *Proc. ICPR'98*, pp. 465–467. IEEE Computer Society, 1998.
9. L.M.J. Florack et al. General Intensity Transformations and Differential Invariants. *Journal of Mathematical Imaging and Vision*, 4(2):171–187, 1994.